Geophysical Research Letters

RESEARCH LETTER
10.1029/2020GL088184

Ocean Tide Loading Effects on InSAR Observations Over Wide Regions

Chen Yu[1], Nigel T. Penna[1], and Zhenhong Li[1,2]

[1]School of Engineering, Newcastle University, Newcastle upon Tyne, UK, [2]College of Geological Engineering and Geomatics, Chang'an University, Xi'an, China

Key Points:
- Ocean tide loading effects can be comparable to long-wavelength tropospheric effects on InSAR observations
- Ocean tide loading corrections reduce the noise level of InSAR time series with more distant pixel pairs receiving larger reduction
- Global ocean tide loading effect maps are generated based on the actual Sentinel-1 acquisition times and dates of all tracks

Supporting Information:
- Supporting Information S1

Correspondence to:
C. Yu,
chen.yu@newcastle.ac.uk

Citation:
Yu, C., Penna, N. T., & Li, Z. (2020). Ocean tide loading effects on InSAR observations over wide regions. *Geophysical Research Letters*, *47*, e2020GL088184. https://doi.org/10.1029/2020GL088184

Received 28 MAR 2020
Accepted 2 JUL 2020
Accepted article online 17 JUL 2020

Abstract Recent and future Interferometric Synthetic Aperture Radar (InSAR) missions provide spatially wide and temporally continuous observations capturing relative ground motions over great distances which enable nationwide or continent-wide deformation mapping. To achieve this, long wavelength errors, which increase with distance and are coupled with geophysical deformation, must be corrected. We predict the ocean tide loading (OTL) effect on Sentinel-1 interferograms globally for all ascending and descending acquisitions, and they are largest in coastal regions. Then, interferograms over southwest Britain are investigated, with the OTL correction having a similar noise reduction effect as when correcting for tropospheric delay (27% standard deviation reduction for tropospheric delay and 46% for combined tropospheric delay and OTL). OTL corrections contribute considerably to the noise reduction of the InSAR time series, with the time series standard deviation reducing by 33% after correcting tropospheric errors and 52% after also applying OTL corrections.

Plain Language Summary Interferometric Synthetic Aperture Radar (InSAR) interferograms provide measurements of Earth's surface deformation at unprecedented detail over areas of tens to now several hundred kilometers with the current Sentinel-1 mission. However, geophysical signals are easily masked in these measurements by errors which increase with distance and exhibit long wavelength effects. One such long wavelength effect is ocean tide loading (OTL), which is negligible over shorter distances (tens of kilometers), but becomes important over several hundred kilometers and has not normally been considered for InSAR. Over 5 years, we evaluate the OTL effect globally on interferograms from Sentinel-1 and suggest substantial contamination arises over most coastal and many tectonically active regions. The OTL correction improves the precision of individual interferograms and contributes considerably to the noise reduction of the InSAR time series. Our results demonstrate the importance of the OTL effect on InSAR measurements for studies such as plate-scale interseismic strain rate accumulation, postseismic relaxation and Glacial Isostatic Adjustment, and on those seeking to generate nationwide or continent-wide deformation products using InSAR. This will soon be even more important, as future InSAR missions (e.g., GEOSAR) may have a spatial extent of over 1,000 km.

1. Introduction

Earth's deformation, ranging from earthquake rupture, volcanic eruption, landslides to groundwater storage variations, may now be mapped anywhere globally at high spatial and temporal resolution over wide regions owing to recent advances in Interferometric Synthetic Aperture Radar (InSAR). For example, the two European Space Agency (ESA) Sentinel-1 satellites map the global landmasses with a 250 km swath width at 5 m by 20 m spatial resolution and a repeat cycle of 6 days (Torres et al., 2012). The planned Geosynchronous SAR (GEOSAR) satellites even have a capacity to provide daily coverage for approximately one third of the globe (Hu et al., 2010). Therefore, as the interest in nationwide or continent-wide deformation mapping grows (e.g., Semple et al., 2017; Zinno et al., 2018), the study of long wavelength deformation signals (spanning over 100 km) that cannot be detected over local scales, such as interseismic tectonic strain accumulation (e.g., Hussain et al., 2018), postseismic relaxation of fault systems (Feng et al., 2016) and Glacial Isostatic Adjustment (GIA) (e.g., Auriac et al., 2014), becomes important. For such studies, long wavelength errors that cannot be eliminated by spatial differencing must therefore be mitigated, with best-fit planes used previously (e.g., Biggs et al., 2007). However, best-fitting planes are not applicable over wider areas since they risk removing some real geophysical signals (Fattahi & Amelung, 2014). Instead, long wavelength errors should be modeled independently in the InSAR processing to avoid the need for

spatial-temporal filters and reduce computational burdens, especially for near-real-time analysis as is needed for mapping and monitoring many geohazards.

Long wavelength errors on InSAR include tropospheric delays, which may be corrected using GPS estimates, numerical weather models, or their combination (e.g., Yu et al., 2018, 2018); ionospheric delays, which for C-band satellites such as Sentinel-1 are nearly negligible (~5.5% of the effect on L band satellites given a similar orbit geometry; Fattahi et al., 2017) or for some extreme situations, such as in low latitudes or polar regions, may be mitigated by the split-spectral technique (Gomba et al., 2016); orbital ramp errors, which can be removed by precise orbit determination from on-board GPS receivers (Peter et al., 2017). Solid earth tide errors have also been suggested by Xu and Sandwell (2019) as needing to be modeled to improve the accuracy of phase unwrapping and to reduce InSAR time series noise.

A further long wavelength effect is ocean tide loading (OTL), caused by the periodic redistribution of ocean water mass which loads and deforms the solid Earth. OTL can vary rapidly both spatially and temporally, and in some parts of the world the crust can be displaced by more than 10 cm in just over 6 hr (Baker, 1984). With OTL deformation having a wavelength that can be an order of magnitude shorter than solid earth tide deformation (e.g., Blewitt, 2007), it follows that for larger spatial InSAR coverage (100–200 km or more) and applications requiring time series such as interseismic strain accumulation and postseismic relaxation, modeling OTL displacement is also now critical. While it has long been recognized that geodetic techniques are susceptible to OTL displacements, including the Global Positioning System (GPS) (e.g., Penna et al., 2007), Satellite Laser Ranging (e.g., Sośnica et al., 2013), and Very Long Baseline Interferometry (e.g., Petrov & Ma, 2003), such OTL displacement corrections have not normally been applied to InSAR measurements.

Displacements caused by OTL on InSAR measurements were first considered by DiCaprio and Simons (2008) on simulating the geometry of the ERS and Envisat satellites, suggesting that a 3 cm per 100 km OTL-induced displacement gradient could arise. Follow on works include Lei et al. (2017) and Peng et al. (2017) who applied OTL corrections to interferograms over Shanghai and Los Angeles. However, it appeared that their results did not adequately demonstrate any sensitivity to the OTL signal. Lei et al. (2017) claimed deformation observations were improved, but no details of the InSAR processing were given. Peng et al. (2017) relied on GPS to remove a bilinear ramp but ignored tropospheric delay effects which could easily mask the OTL signal. Their interferograms also contained only small OTL signals compared with other error sources such as orbital errors which dominated. Furthermore, the effect of OTL on InSAR time series was not investigated.

In light of the increasing interest in mapping long wavelength deformation processes and the lack of demonstration of OTL effects on actual InSAR measurements and time series, in this paper we investigate the spatial-temporal effects of OTL displacement on Sentinel-1 InSAR. We first provide global simulation maps of where such effects are likely to be important. We then consider a study area to demonstrate the sensitivity to and importance of modeling OTL displacement (together with tropospheric delay effects), both on individual interferograms and their time series. We aim to demonstrate the importance of the OTL effect for the abovementioned tectonic and GIA studies and the generation of nationwide or continent-wide deformation products using InSAR.

2. Predicted OTL Effects on Global InSAR Observations

To provide a global indication of the OTL effect on Sentinel-1 interferograms and resulting time series, we show in Figure 1a the distribution of standard deviations (StdDev) of line-of-sight (LOS) predicted OTL displacement time series, using all 12-day observational epochs for both ascending and descending tracks from the first acquisition epoch after the July 2014 start of mission to end of December 2020. For a 0.25° grid, the modeled east, north, and vertical OTL displacements were computed at each observational epoch by inputting 11 constituents of the FES2014b ocean tide model (Carrère et al., 2016) to the NLOADF software (Agnew, 1997) with a PREM (Dziewonski & Anderson, 1981) elastic Green's function, and then to the IERS Conventions 2010 (Petit & Luzum, 2010) hardisp routine. The component displacements were projected to LOS using the average incidence (~39°) and heading angles (−15° for ascending and −166° for descending tracks, respectively) of the interferograms to form, per 0.25° grid point, the LOS time series and its StdDev, computed as

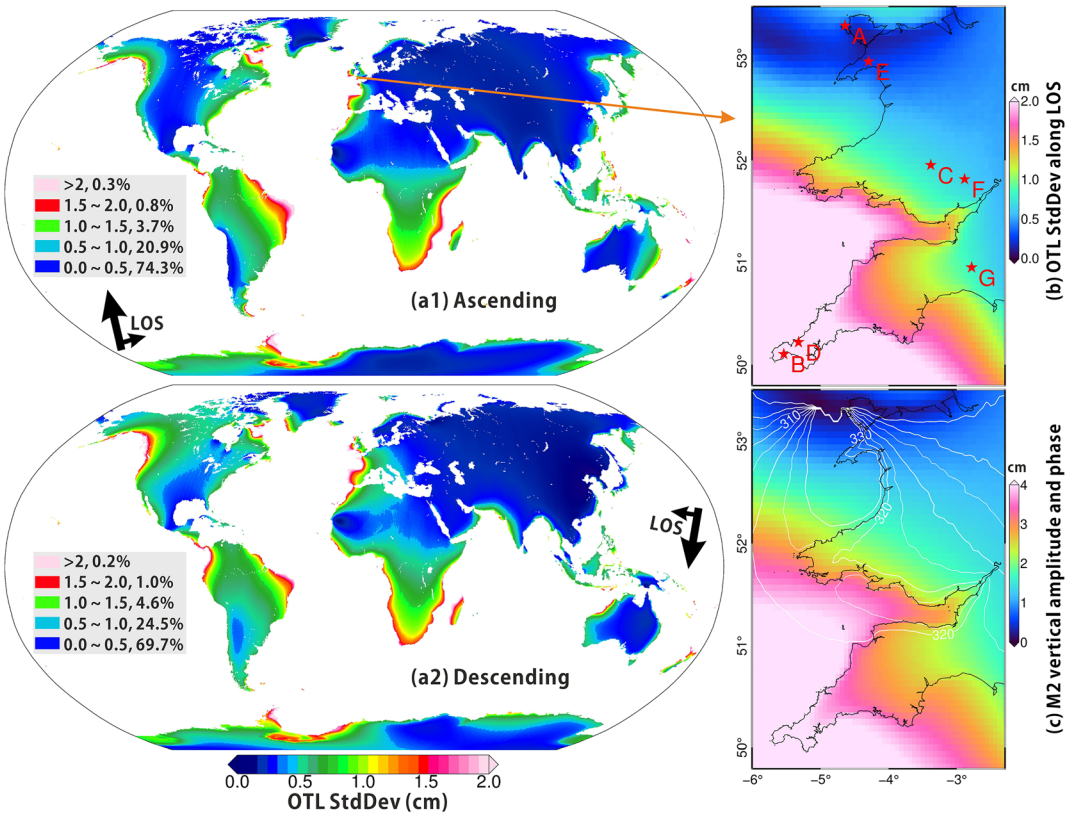

Figure 1. (a) FES2014b global predicted OTL displacement 12-day time series StdDev (Equation 1) along LOS for Sentinel-1 ascending (a1) and descending (a2) tracks from the beginning of the mission to December 2020. (b) As in (a1) but for southwest Britain. (c) FES2014b predicted M_2 vertical OTL amplitude and Greenwich phase lag (degrees) for southwest Britain.

$$StdDev_{OTL} = \sqrt{\frac{1}{n-1}\sum_{i=1}^{n}\left(OTL_i - \overline{OTL}\right)^2} \tag{1}$$

where OTL_i is the predicted LOS OTL displacement at 12-day observational epoch i; n is the number of epochs; $\overline{OTL}$ is the mean LOS OTL displacement of the whole time series. Figure 1a shows that the largest LOS StdDevs (>2 cm) occur for coastal regions, including western Europe, east Brazil, southeast Africa, Gulf of Alaska, northwest Australia, New Zealand, and the Antarctic Peninsula. At some locations hundreds of kilometers inland, such as central Russia, the StdDev is less than 0.5 cm.

Of the multiple harmonic constituents which are summed to represent the total OTL displacement, M_2 is largest in most parts of the world (e.g., Agnew, 2007), and the spatial variation in the global displacement StdDevs shown in Figure 1 is largely influenced by the M_2 vertical OTL displacement amplitude. Maps of the east, north, and vertical component OTL displacement amplitude and phase lag global distributions are provided for M_2 and also the largest diurnal constituents (K_1 and O_1) in the supporting information. While the S_2 constituent is typically the next largest semidiurnal constituent after M_2, the 6- and 12-day repeat sampling of the Sentinel-1 satellites mean it is almost entirely aliased to a constant displacement, so has negligible effect on InSAR processing. Except around the Gulf of Alaska and the Arabian and Weddell Seas, K_1 is much smaller than M_2 and therefore contributes much less to the LOS StdDev values shown in Figure 1a.

Both the OTL displacement magnitude and spatial gradient must be considered for evaluating the effects of OTL on InSAR, with Figure 1a showing that particularly large and nonlinear LOS StdDev spatial gradients occur for parts of western Europe and New Zealand. The Figure 1b LOS StdDev enlargement exemplifies that southwest Britain has some of the largest and most spatially variable LOS OTL displacements in the

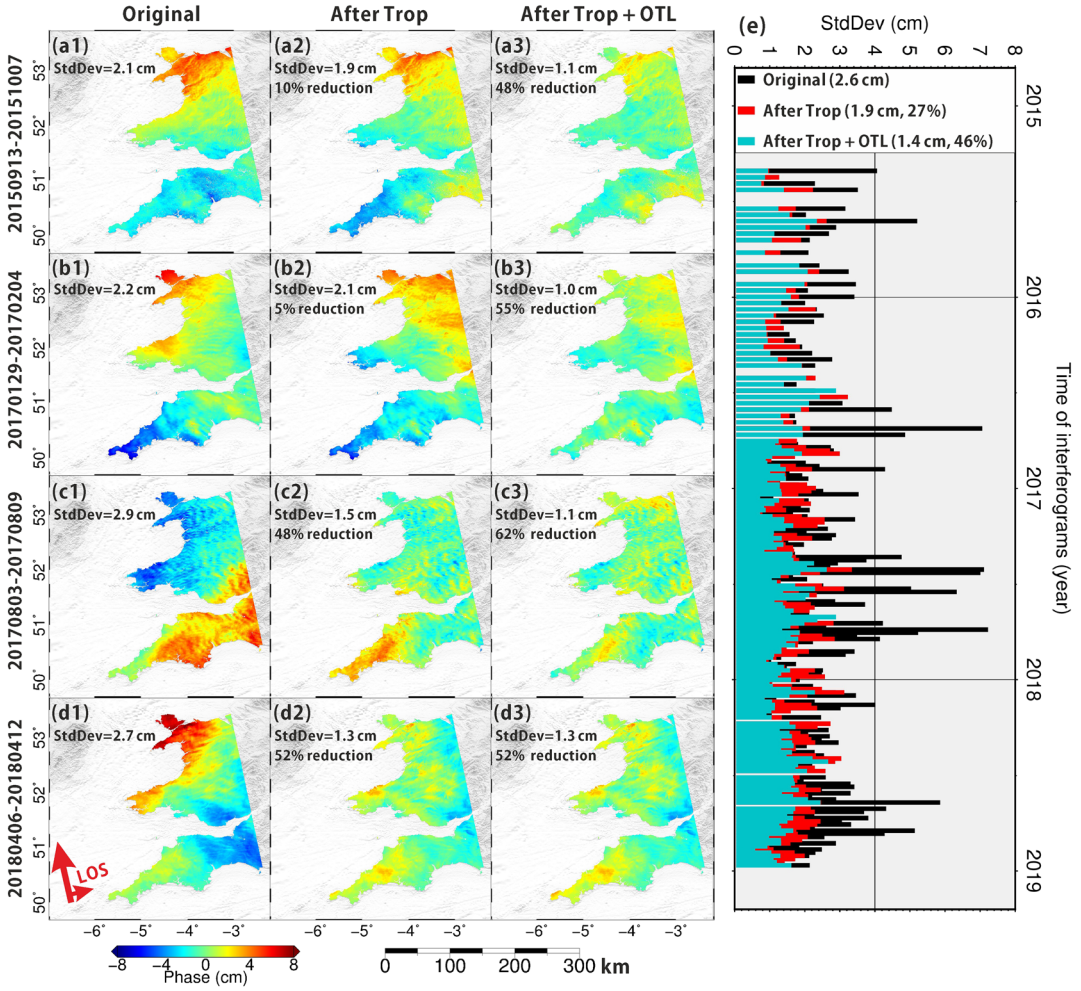

Figure 2. Four examples of the original (a1, b1, c1, and d1), tropospheric corrected (a2, b2, c2, and d2), and tropospheric and OTL corrected Sentinel-1 interferograms (a3, b3, c3, and d3), with their respective LOS StdDev values listed. Panel (e) shows the corresponding LOS StdDev values for all 170 consecutive interferograms over time, with the mean of the StdDevs listed.

world, and therefore the region was chosen to assess the impact of OTL corrections on InSAR. As seen from Figure 1b and also the M_2 vertical amplitude and Greenwich phase lag plots in Figure 1c, there is a notable decrease in OTL displacement from the southwest (2.5 cm LOS StdDev and 4–5 cm M_2 vertical amplitude in Cornwall) to northeast (~0.5 cm LOS StdDev and few mm M_2 vertical amplitude in north Wales). Regarding the accuracy of the predicted OTL displacement over southwest Britain, Bos et al. (2015) compared predicted M_2 OTL vertical displacements with GPS estimates across western Europe which encompassed our study area, and obtained a 0.7 mm mean difference and a maximum difference of 2.8 mm.

Using the GAMMA software and ESA orbits for removing long wavelength orbital ramps, we processed a series of 170 independent Sentinel-1 interferograms extending ~250 km by ~380 km (Figure 2) from May 2015 to December 2018. A spatial multilook filter was applied to reduce phase noise, leading to an interferogram resolution of about 90 m. For the epochs of each interferogram, we applied the OTL displacement per pixel after bilinear interpolation from a 0.0625° LOS OTL displacement computed grid. The tropospheric correction was modeled per pixel using the Generic Atmospheric Correction Online Service for InSAR (GACOS, http://ceg-research.ncl.ac.uk/v2/gacos/), which utilizes the European Centre for Medium-Range Weather Forecasts high-resolution numerical weather model and removes the long wavelength and the elevation dependent tropospheric delays on InSAR measurements (Yu et al., 2017; Yu, Li, Penna, & Crippa, 2018).

Throughout this manuscript, we use the displacement measurement StdDev to describe the quality of the interferograms. A lower-displacement StdDev across the whole interferogram indicates fewer spatially long wavelength errors and a lower-displacement time series StdDev indicates less noisy and more temporally stable measurements. Therefore, another reason to choose southwest Britain as the study area is that it is a tectonically inactive region (Bird & Kreemer, 2015; Gutmanis et al., 1991; Helffrich et al., 2003) which avoids introducing errors caused by permanent deformation.

3. OTL Correction on Individual Interferograms

Figure 2 shows some example interferograms that are original, corrected for tropospheric delay only, and corrected for both tropospheric delay and OTL. The original interferograms experience extensive errors owing to their wide coverage, which are substantially reduced on applying the tropospheric corrections. However, considerable long wavelength residuals remain, with Figure 2 showing how three of the troposphere-corrected interferograms exhibit signals with long wavelength from southwest to northeast similar to the predicted OTL displacement shown in Figure 1, but which are masked in the original interferograms. After also applying OTL corrections, these long wavelength signals are almost entirely eliminated. The magnitude of OTL errors on the interferograms can be comparable with tropospheric delays, with Figures 2a–2c denoting how only correcting for tropospheric delay accounts for 10%, 5%, and 48% reductions in the respective StdDev values, but if OTL is also included the reductions are 48%, 55%, and 62%, respectively. Figure 2d is an example whereby applying OTL corrections results in minimal interferogram error reductions, because the two images were collected at times when the periodic OTL displacement was close to zero, and the majority of error reduction for this case comes from applying the tropospheric corrections.

Figure 2e shows the StdDev reduction for all 170 consecutive interferograms from May 2015 to December 2018. The original interferograms show a fluctuating StdDev over time with 19 exceeding 4 cm. After applying the tropospheric corrections, the StdDev values become more stable over time, with the mean StdDev reducing from 2.6 to 1.9 cm (27% improvement). Applying also the OTL corrections further reduces the mean StdDev to 1.4 cm, corresponding to a 46% improvement over the original. This implies that for this region, correcting the OTL signal is of similar importance to the tropospheric delay for reducing measurement noise and to subsequently interpret millimeter or centimeter level deformation signals.

4. OTL Correction on Interferogram Time Series

Having obtained substantial noise reductions on individual interferograms after applying OTL corrections, we further investigated OTL effects using InSAR time series. We first estimated the mean linear velocity of each pixel using interferogram stacking (e.g., Lyons & Sandwell, 2003), using the average phase rate of the 170 interferograms. We then computed the StdDev of the detrended time series residuals per pixel. The displacement time series was constructed using the consecutive interferograms without any spatial-temporal filters (e.g., Albino et al., 2019), which is computationally efficient and therefore suitable for near-real-time processing applications. We did not apply more sophisticated time series analysis methods such as persistent scatterer (Hooper et al., 2004) or small baseline (Mora et al., 2002) as they rely on strong spatial-temporal filters, are more suited to extracting more localized deformation signals, and require extensive computational resources for the large spatial extent considered here.

Figures 3a and 3b respectively show the mean velocity maps estimated from the interferograms that are original or have had tropospheric or tropospheric+OTL corrections applied and the maps of the StdDev of the residuals after the velocity estimation. The original velocity estimates exhibit the largest variation across the image with a mean residual StdDev of 3.7 cm and velocities of over 10 cm/year in two areas highlighted in red circles, which could be falsely interpreted as ground deformation. Since the OTL signal is largely periodic, its effect on the mean velocity estimation is minimized by averaging, leaving the tropospheric delay dominant (Figures 3a2 and 3a3). However, the OTL correction substantially reduces the estimation uncertainty: the original residual StdDev of 3.7 cm reduces to 2.5 cm after applying tropospheric corrections then further to 2.1 cm after applying both tropospheric and OTL corrections, corresponding to 32% and 43%

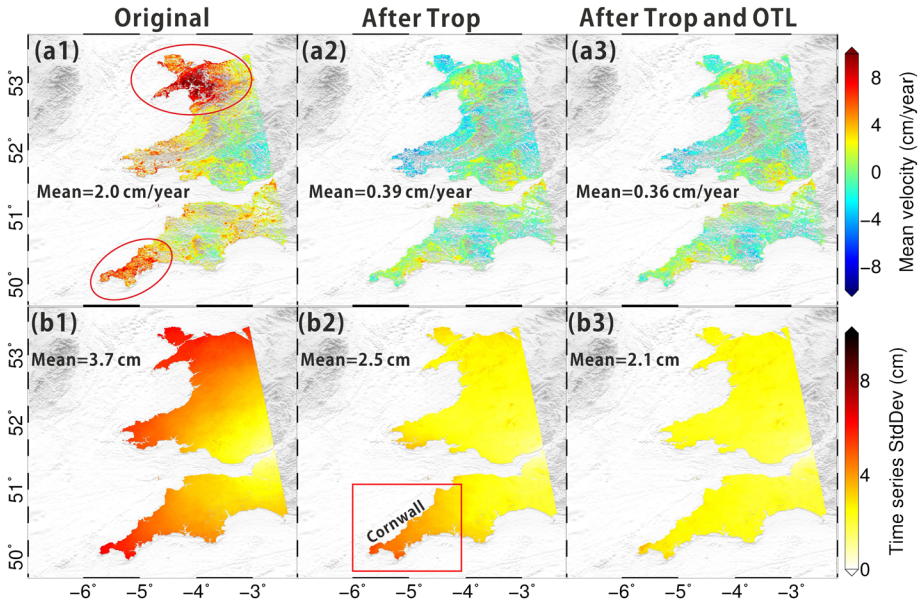

Figure 3. Mean LOS velocity maps and their residual time series StdDev maps estimated using the original Sentinel-1 interferograms (a1, b1), tropospheric-corrected interferograms (a2, b2), and tropospheric+OTL-corrected interferograms (a3, b3), respectively.

respective reductions. In particular, over Cornwall (Figure 3b2, red box), most of the StdDsev reductions arise from the OTL corrections.

To further investigate the noise reduction observed in Figure 3b, we consider some example pixel pairs and plot in Figure 4a six displacement baseline time series at different separation distances and azimuths, between the locations marked on Figure 1b. Due to the long wavelength nature of the OTL signal, the noise reduction after applying OTL corrections is distance dependent, with the medium-to-long separation pairs receiving greater noise reduction than the short separation pairs. For example, the StdDev of pair A-B, separated by 363 km and with a 4 cm M_2 vertical OTL amplitude difference between locations A and B, reduces from 5.7 cm to 1.9 cm after applying tropospheric+OTL corrections, compared with 3.7 cm when only the tropospheric correction is applied. Whereas for the 20 km separation distance pair D-B, the contribution of the OTL corrections is negligible. The OTL effect is also azimuth dependent, for example, pairs A-G and C-B have a similar separation distance but the contribution of OTL corrections for pair C-B (1.0 cm StdDev reduction) is much larger than A-G (0.3 cm StdDev reduction), which matches the respective differing gradients of OTL displacement LOS StdDev and M_2 vertical amplitude shown in Figure 1.

Examining further the tropospheric-corrected time series for baselines A-B and C-B in Figure 4b, distinct cyclic effects can be seen, which are very similar to the modeled LOS OTL displacement time series superimposed: the correlations between the model and the observations for the respective baselines are 0.88 and 0.77. For both baselines A-B and C-B, spectral analysis of the LOS tropospheric-corrected displacement time series from May 2015 to October 2016 (points every 12 days) and from October 2016 to December 2018 (points every 6 days) revealed the dominant signals had periods of 64 and 14.8 days, respectively, which match those from respective 12- and 6-day aliasing of the M_2 harmonic (Xu & Sandwell, 2019). This further confirms the sensitivity of the InSAR data to OTL effects, and that the M_2 constituent is dominant over this region.

To further investigate the noise reduction spatial dependency after applying OTL corrections, we display in Figure 4c spatial structure functions (as per Li et al., 2006) highlighting anisotropy for the original and the two corrected InSAR time series. The value of each pixel in Figure 4c together with its specific distance and azimuth from the origin (coordinates 0,0 km) represents the average time series noise level (StdDev) of all pixel pairs from all interferograms in the original or corrected time series which are separated by that distance and azimuth. Also labeled in Figure 4c are the overall means of these pixel pair StdDev values.

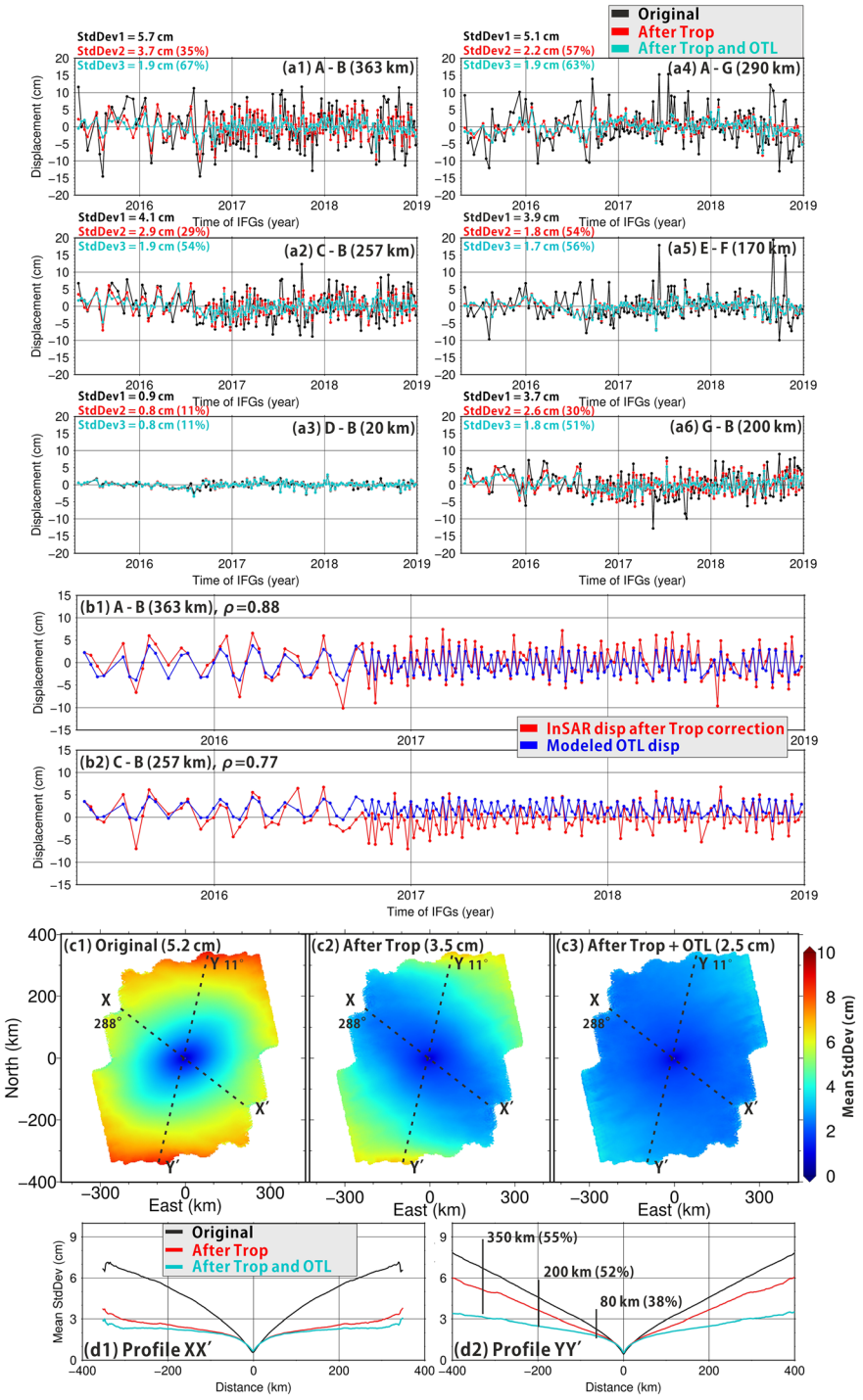

Figure 4. (a1–a6) Sentinel-1 InSAR LOS time series at different separation distances and azimuths for pixel pairs displayed in Figure 1b, with (b1, b2) showing a comparison with the modeled OTL displacement for two pixel pairs. Panels (c1)–(c3) shows the mean StdDev at specific distances and azimuths referenced to the center, representing the averaged time series noise level of pixel pairs on interferograms (IFGs) separated by that distance and azimuth. (d1, d2) Profiles for the three maps in panels (c1–c3).

Figure 4c1 reveals that the original interferogram time series has a low noise level for pixels less than 50 km apart, then beyond this the StdDev increases nearly proportionally with the separation distance. The effect of the OTL signal is small along the direction of profile XX', with the tropospheric correction contributing over

90% of the overall noise reduction. However, for the profile YY' (along 11° azimuth) where the original time series is noisiest, it can be seen from Figures 4c2 and 4d2 that the tropospheric correction is largely insufficient. Instead, most of the noise reduction arises from the OTL correction, accounting for over 50% when the separation distance exceeds 200 km. The 11° azimuth of the noisiest profile is also consistent with the southwest to northeast gradient of the LOS OTL per pixel StdDev and the M_2 vertical OTL amplitude shown in Figure 1. The overall StdDev reduces from 5.2 to 3.5 cm on applying the tropospheric corrections (33% reduction), and to 2.5 cm when also correcting for OTL (52% reduction), providing further evidence of the sensitivity of InSAR time series to OTL.

5. Conclusions and Outlook

We have shown that OTL displacement can have substantial effects on Sentinel-1 InSAR measurements, particularly over medium-to-long distances (~100–400 km) where its displacement magnitude can be comparable to that caused by tropospheric delays. Mean StdDev reductions from tropospheric effects on individual interferograms were 27% over 3.5 years, increasing to 46% when OTL corrections were also included. For two example baselines separated by more than 250 km, the OTL corrections reduced the noise level of the InSAR LOS time series by over 50%, with the amount of reduction generally increasing with baseline length, although it also depended on the azimuth of the OTL displacement gradient. Applying OTL corrections in addition to tropospheric delays resulted in an overall InSAR time series StdDev reduction of 52% (33% reduction with only tropospheric delays) which is crucial for velocity mapping and the investigation of time varying deformation processes over large spatial extents (few hundred kilometers or more). These time series results were computed without applying any spatial-temporal filters, implying that, along with tropospheric error corrections, applying OTL corrections before the time series analysis helps to reduce the computational requirement. This is essential for recent and future InSAR applications, particularly for near-real-time deformation monitoring.

The OTL effect on InSAR measurements has been shown to be dependent on the magnitude (constituent amplitude and time series displacement StdDev) and spatial gradient of the OTL displacement. For the southwest Britain interferogram extent considered (~250 km by 380 km), the LOS StdDev varies nonlinearly from 2.5 cm to under 0.5 cm, and correcting for such large and variable OTL displacement will aid estimates of GIA from Sentinel-1 interferograms. The global predicted OTL StdDev maps suggest that Sentinel-1 GIA estimates will also be improved by applying OTL corrections for the rest of Britain, Ireland, northeast Canada, and southwest Greenland, where large StdDev values and gradients also arise. Similarly, several tectonically active regions such as Alaska, western California, New Zealand, Japan, southeast Asia, Central America, northeastern South America are identified as areas where OTL effects are substantial, with an average LOS StdDev of ~2.0 cm, implying that the correction of the OTL signal will improve long wavelength interseismic and postseismic deformation mapping in these coastal areas. Some inland areas are also affected, with most of western North America, southern Africa and most of South America experiencing 1.5–2.0 cm StdDev. Meanwhile, due to different satellite geometries, parts of eastern and southern Asia have larger OTL effects on Sentinel-1 ascending tracks than descending tracks, whereas the west coast of Europe and most of North America have larger effects on descending tracks.

This paper has considered OTL effects on Sentinel-1 for southwest Britain and identified where else globally the effects are likely to be important. Similar LOS OTL displacement time series StdDev maps may be generated for other InSAR data sets such as ALOS-2 and TerraSAR-X, especially for future missions such as GEOSAR which has a much wider coverage aiming for nationwide or continent-wide products. However, as the StdDev magnitudes and spatial variation are largely governed by the M_2 OTL vertical displacement amplitude and phase lag variations, the same regions as discussed herein are also likely to be where OTL displacement corrections mostly need to be considered. Finally, to readily enable InSAR users to model OTL effects, we plan to make OTL corrections available via GACOS.

Data Availability Statements

The Sentinel-1 data were obtained from ESA (https://scihub.copernicus.eu/dhus/#/home), and the ECMWF data were obtained from this site (https://apps.ecmwf.int/archive-catalogue/?type=an&class=od&stream=oper&expver=1).

Acknowledgments

Thanks to Duncan Agnew for providing the SPOTL (https://igppweb.ucsd.edu/~agnew/Spotl/spotlmain.html) and hardisp softwares, and AVISO for FES2014b. This work was supported by the UK NERC through the Centre for the Observation and Modelling of Earthquakes, Volcanoes and Tectonics (COMET, Ref.: come30001) and the LICS project (Ref. NE/K010794/1), and the European Space Agency through the ESA-MOST DRAGON-4 project (Ref.: 32244). Part of the work was also supported by the Natural Science Foundation of China (ref.: 41941019).

References

Agnew, D. C. (1997). NLOADF: A program for computing ocean-tide loading. *Journal of Geophysical Research*, *102*(B3), 5109–5110. https://doi.org/10.1029/96jb03458

Agnew, D. C. (2007). Earth tides. In T. A. Herring (Ed.), *Treatise on geophysics and geodesy*. (pp. 163–195). New York: Elsevier. https://doi.org/10.1016/B978-044452748-6.00056-0

Albino, F., Biggs, J., & Syahbana, D. K. (2019). Dyke intrusion between neighbouring arc volcanoes responsible for 2017 pre-eruptive seismic swarm at Agung. *Nature Communications*, *10*(1), 748. https://doi.org/10.1038/s41467-019-08564-9

Auriac, A., Sigmundsson, F., Hooper, A., Spaans, K. H., Björnsson, H., Pálsson, F., et al. (2014). InSAR observations and models of crustal deformation due to a glacial surge in Iceland. *Geophysical Journal International*, *198*(3), 1329–1341. https://doi.org/10.1093/gji/ggu205

Baker, T. (1984). Tidal deformations of the Earth. *Science Progress*, *69*, 197–233.

Biggs, J., Wright, T., Lu, Z., & Parsons, B. (2007). Multi-interferogram method for measuring interseismic deformation: Denali Fault, Alaska. *Geophysical Journal International*, *170*(3), 1165–1179. https://doi.org/10.1111/j.1365-246X.2007.03415.x

Bird, P., & Kreemer, C. (2015). Revised tectonic forecast of global shallow seismicity based on version 2.1 of the global strain rate map. *Bulletin of the Seismological Society of America*, *105*(1), 152–166. https://doi.org/10.1785/0120140129

Blewitt, G. (2007). Chapter in treatise on geophysics. In G. Schubert (Ed.), *GPS and space-based geodetic methods*. (pp. 351–390). Oxford: Academic Press.

Bos, M. S., Penna, N. T., Baker, T. F., & Clarke, P. J. (2015). Ocean tide loading displacements in western Europe: 2. GPS-observed anelastic dispersion in the asthenosphere. *Journal of Geophysical Research: Solid Earth*, *120*, 6540–6557. https://doi.org/10.1002/2015JB011884

Carrère, L., Lyard, F., Cancet, M., Guillot, A., & Picot, N. (2016). FES 2014, a new tidal model—Validation results and perspectives for improvements, In: Proceedings of the ESA Living Planet Symposium. pp. 9–13. https://doi.org/https://www.aviso.altimetry.fr/

DiCaprio, C. J., & Simons, M. (2008). Importance of ocean tidal load corrections for differential InSAR. *Geophysical Research Letters*, *35*, L22309. https://doi.org/10.1029/2008GL035806

Dziewonski, A. M., & Anderson, D. L. (1981). Preliminary reference Earth model. *Physics of the Earth and Planetary Interiors*, *25*(4), 297–356. https://doi.org/10.1016/0031-9201(81)90046-7

Fattahi, H., & Amelung, F. (2014). InSAR uncertainty due to orbital errors. *Geophysical Journal International*, *199*(1), 549–560. https://doi.org/10.1093/gji/ggu276

Fattahi, H., Simons, M., & Agram, P. (2017). InSAR time-series estimation of the ionospheric phase delay: An extension of the split range-spectrum technique. *IEEE Transactions on Geoscience and Remote Sensing*, *55*(10), 5984–5996. https://doi.org/10.1109/TGRS.2017.2718566

Feng, W., Samsonov, S., Li, P., & Omari, K. (2016). Coseismic and early-postseismic displacements of the 2015 MW8.3 Illapel (Chile) earthquake imaged by Sentinel-1a and RADARSAT-2, In: International Geoscience and Remote Sensing Symposium (IGARSS). IEEE, pp. 5990–5993. https://doi.org/10.1109/IGARSS.2016.7730565

Gomba, G., Parizzi, A., De Zan, F., Eineder, M., & Bamler, R. (2016). Toward operational compensation of ionospheric effects in SAR interferograms: The split-spectrum method. *IEEE Transactions on Geoscience and Remote Sensing*, *54*(3), 1446–1461. https://doi.org/10.1109/TGRS.2015.2481079

Gutmanis, J. C., Hailwood, E. A., Maddock, R. H., & Vita-Finzi, C. (1991). The use of dating techniques to constrain the age of fault activity: A case history from north Somerset, United Kingdom. *The Quarterly Journal of Engineering Geology*, *24*(4), 363–374. https://doi.org/10.1144/GSL.QJEG.1991.024.04.04

Helffrich, G., Asencio, E., Knapp, J., & Owens, T. (2003). Transition zone structure in a tectonically inactive area: 410 and 660 km discontinuity properties under the northern North Sea. *Geophysical Journal International*, *155*(1), 193–199. https://doi.org/10.1046/j.1365-246X.2003.02036.x

Hooper, A., Zebker, H., Segall, P., & Kampes, B. (2004). A new method for measuring deformation on volcanoes and other natural terrains using InSAR persistent scatterers. *Geophysical Research Letters*, *31*, L23611. https://doi.org/10.1029/2004GL021737

Hu, C., Zeng, T., Zhu, Y., & Ding, Z. (2010). The accurate resolution analysis in geosynchronous SAR, in: Proceedings of the European conference on synthetic aperture radar, EUSAR. pp. 925–928.

Hussain, E., Wright, T. J., Walters, R. J., Bekaert, D. P. S., Lloyd, R., & Hooper, A. (2018). Constant strain accumulation rate between major earthquakes on the North Anatolian Fault. *Nature Communications*, *9*(1), 1392. https://doi.org/10.1038/s41467-018-03739-2

Lei, M., Wang, Q., Liu, X., Xu, B., & Zhang, H. (2017). Influence of ocean tidal loading on InSAR offshore areas deformation monitoring. *Geodesy and Geodynamics*, *8*(1), 70–76. https://doi.org/10.1016/j.geog.2016.09.004

Li, Z., Fielding, E. J., Cross, P., & Muller, J. P. (2006). Interferometric synthetic aperture radar atmospheric correction: GPS topography-dependent turbulence model. *Journal of Geophysical Research*, *111*, B02404. https://doi.org/10.1029/2005JB003711

Lyons, S., & Sandwell, D. (2003). Fault creep along the southern San Andreas from interferometric synthetic aperture radar, permanent scatterers, and stacking. *Journal of Geophysical Research*, *108*(B1), 2047. https://doi.org/10.1029/2002jb001831

Mora, O., Lanari, R., Mallorqui, J. J., Berardino, P., & Sansosti, E. (2002). A new algorithm for monitoring localized deformation phenomena based on small baseline differential SAR interferograms, in: IEEE International Geoscience and Remote Sensing Symposium. pp. 1237–1239. https://doi.org/10.1109/IGARSS.2002.1025900

Peng, W., Wang, Q., & Cao, Y. (2017). Analysis of ocean tide loading in differential InSAR measurements. *Remote Sensing*, *9*(2), 101. https://doi.org/10.3390/rs9020101

Penna, N. T., King, M. A., & Stewart, M. P. (2007). GPS height time series: Short-period origins of spurious long-period signals. *Journal of Geophysical Research*, *112*, B02402. https://doi.org/10.1029/2005JB004047

Peter, H., Jäggi, A., Fernández, J., Escobar, D., Ayuga, F., Arnold, D., et al. (2017). Sentinel-1A – First precise orbit determination results. *Advances in Space Research*, *60*(5), 879–892. https://doi.org/10.1016/j.asr.2017.05.034

Petit, G., & Luzum, B. (2010). IERS Conventions (2010). Bur. Int. Des Poids Mes. Sevres 1–179.

Petrov, L., & Ma, C. (2003). Study of harmonic site position variations determined by very long baseline interferometry. *Journal of Geophysical Research*, *108*(B4). https://doi.org/10.1029/2002jb001801

Semple, A. G., Pritchard, M. E., & Lohman, R. B. (2017). An incomplete inventory of suspected human-induced surface deformation in North America detected by satellite interferometric synthetic-aperture radar. *Remote Sensing*, *9*(12). https://doi.org/10.3390/rs9121296

Sośnica, K., Thaller, D., Dach, R., Jäggi, A., & Beutler, G. (2013). Impact of loading displacements on SLR-derived parameters and on the consistency between GNSS and SLR results. *Journal of Geodesy*, *87*(8), 751–769. https://doi.org/10.1007/s00190-013-0644-1

Torres, R., Snoeij, P., Geudtner, D., Bibby, D., Davidson, M., Attema, E., et al. (2012). GMES Sentinel-1 mission. *Remote Sensing of Environment*, *120*, 9–24. https://doi.org/10.1016/j.rse.2011.05.028

Xu, X., & Sandwell, D. T. (2019). Toward absolute phase change recovery with InSAR: Correcting for earth tides and phase unwrapping ambiguities. *IEEE Transactions on Geoscience and Remote Sensing*, *58*(1), 726–733. https://doi.org/10.1109/tgrs.2019.2940207

Yu, C., Li, Z., & Penna, N. T. (2018). Interferometric synthetic aperture radar atmospheric correction using a GPS-based iterative tropospheric decomposition model. *Remote Sensing of Environment*, *204*, 109–121. https://doi.org/10.1016/j.rse.2017.10.038

Yu, C., Li, Z., Penna, N. T., & Crippa, P. (2018). Generic atmospheric correction model for interferometric synthetic aperture radar observations. *Journal of Geophysical Research: Solid Earth*, *123*, 9202–9222. https://doi.org/10.1029/2017JB015305

Yu, C., Penna, N. T., & Li, Z. (2017). Generation of real-time mode high-resolution water vapor fields from GPS observations. *Journal of Geophysical Research: Solid Earth*, *122*, 2008–2025. https://doi.org/10.1002/2016JD025753

Zinno, I., Bonano, M., Buonanno, S., Casu, F., De Luca, C., Lanari, R., et al. (2018). Surface deformation mapping of Italy through the P-SBAS dinsar processing of sentinel-1 data in a cloud computing environment, in: International Geoscience and Remote Sensing Symposium (IGARSS). Institute of Electrical and Electronics Engineers Inc., pp. 2241–2243. https://doi.org/10.1109/IGARSS.2018.8519551